Superconducting heterostructure with barrier with strong spin-orbit interaction

Superconducting heterostructure with barrier with strong spin-orbit interaction

K Y Constantinian[1], A M Petrzhik[1], G A Ovsyannikov[1], A V Shadrin[1,2], Yu V Kislinskii[1], G Cristiani[3], and G Logvenov[3]

[1] Kotel'nikov Institute of Radio Engineering and Electronics RAS, Moscow, 125009, Russia
[2] Moscow Institute of Physics and Technology, Dolgoprudny, Moscow Region, 141701, Russia
[3] Max Planck Institute for Solid State Research, Stuttgart, 70569, Germany

E-mail: karen@hitech.cplire.ru

Abstract. We report on observation of superconducting current and AC Josephson effect in mesa-heterostructures with spin-singlet superconducting electrodes, interlayered by a barrier material with strong spin-orbit interaction. The mesa-heterostructures were Nb/Au/Sr_2IrO_4/$YBa_2Cu_3O_x$ with d=5 nm and 7 nm thick interlayer of strontium iridate Sr_2IrO_4, which is known as a canted antiferromagnetic insulator with a weak magnetic moment from Ir atoms and with spin-orbit interaction energy E_{SO}~0.4 eV. The superconducting critical current density was $j_C \approx 0.3$ A/cm^2 at T=4.2 K for mesa-heterostructures with d=7 nm and a few times higher for d=5 nm. The zero-bias conductance peak has been observed due to low energy states originated at Sr_2IrO_4/$YBa_2Cu_3O_x$ interface. Under influence of weak magnetic field the critical current $I_C(H)$ dependences showed Fraunhofer-like pattern indicating absence of pinholes, supported also by oscillating with microwave power Shapiro steps. Fiske resonance steps with voltage positions deviated from the ordinary ones were registered for mesas with d=5 nm.

1. Introduction

In recent years Josephson junctions featuring spin-dependent processes attract increasing interest. Particularly, spin-orbit interaction (SOI) in ferromagnetic (F) barrier material may lead to generation of spin-triplet superconducting current [1-5]. Theoretically magneto-electric effect and spin-triplet pairing were predicted for the case when ferromagnetic interlayer F was replaced by the normal-metal N with SOI [6, 7]. However, most of experimental investigations of impact of SOI on Josephson effect were performed in structures with superconductors linked by a topological insulator. A possibility to replace the topological insulator with a semiconductor film with SOI was suggested in [8] stimulating extensive theoretical and experimental studies [9, 10]. A promising choice of material with strong SOI for superconducting junction is the 5d transition-metal oxide Sr_2IrO_4 [11, 12]. This compound is known as a canted antiferromagnetic insulator with the band splitting, characterized by energy 0.4 eV [13]. Unconventional properties of Sr_2IrO_4 and the interfaces with other oxides, particularly with the superconducting cuprate, are discussed in refs. [14-16]. Moreover, Sr_2IrO_4 gives opportunities [17, 18] for spin manipulation in a junction with the barrier material with weak magnetic moment. For experimental studies a sandwich-type structure seems promising due to the possibility to reduce the

distance between superconductors down to a few nanometers that is necessary for the interference of superconducting wave functions in the junction. An inclusion of high-Z metallic Pt into the ferromagnetic interlayer for experimental study of impact of SOI on superconducting proximity effect was reported in [19].

In this report we present experimental results on observation of superconducting current and study of electron and microwave transport characteristics of hybrid superconducting Nb/Au/Sr_2IrO_4/$YBa_2Cu_3O_x$ sandwich-type mesa-structures with 5 and 7 nm thickness of the Sr_2IrO_4 interlayer.

2. Samples and measurements

For sample fabrication the bilayer of $YBa_2Cu_3O_x$ (YBCO) and Sr_2IrO_4 (SIO) with thickness 60–70 nm and 5–7 nm, correspondingly, were grown epitaxially by pulsed-laser deposition (PLD) on (110) $NdGaO_3$ (NGO) single-crystalline substrates. A KrF-excimer laser with frequency 10 Hz and energy density 1.6 J/cm^2 was used to ablate materials from YBCO and SIO stoichiometric targets. The bottom YBCO thin film was deposited at 830 °C in oxygen atmosphere at pressure of 0.5 mbar. The SIO film was deposited at 700 °C in argon atmosphere with pressure 0.5 mbar. Both YBCO and SIO films were grown with the *c*-axis perpendicular to the substrate plane [16]. A protective Au thin film with thickness about 10 nm was deposited *in situ* at 30 °C in the PLD chamber. The superconducting Nb film with thickness about 200 nm was deposited *ex situ* by magnetron sputtering in an argon atmosphere at room temperature, followed after the sputtering of Au film [20]. The crystalline parameters of the SIO film and the bilayer SIO/YBCO were determined using the four-circle x-ray diffractometer [15, 21]. XRD data show that the lattice parameter c=1.283 nm was obtained for SIO films with thickness 17 nm and c=11.66 nm for YBCO film. Nb/Au/SIO/YBCO mesa-structures (MS) with square shape and sizes A=WL=10x10 to 50x50 μm^2 (total 5 MS on a chip) were formed using optical lithography, reactive ion-plasma etching and ion-beam etching at low ion accelerating voltages. Oxygen plasma treatments were performed after each lithography process in order to remove the remains of the resist. The SiO_2 protective insulator layer was deposited by RF sputtering providing the DC current to flow in perpendicular direction to the MS layers. An additional Nb (or NbN) film with a thickness of 200 nm was sputtered providing superconducting current transport through the DC wiring. Contact pads were made of gold films for 4-point *I-V* curve measurements (see figure 1).

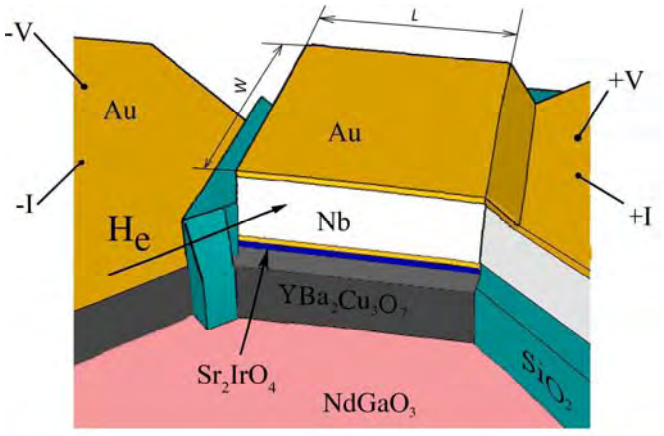

Figure 1. A sketch of 3D view of the mesa-heterostructure Nb/Au/SIO/YBCO on $NdGaO_3$ substrate. The in-plane external magnetic field H_e was applied as showed by the arrow. The insulating SiO_2 layer separates top and bottom electrodes and provides electrical transport along the *c*-axis. Four-probe current supply and voltage measurement wires connected to the separated Au contact pads are shown schematically. *Adapted from* [21].

3. Results and discussion

3.1. DC characteristics of MS

Temperature dependence of resistance $R(T)$ for MS is shown in figure 2a. Although the temperature dependences of resistivity of the reference SIO film had an activated character at relatively high temperatures [16] the resistances of Nb and YBCO electrodes gave the main contribution to R. After Nb-wiring pattering the transition temperature of the YBCO electrode in the MS has reduced to $T_{C\_YBCO} \approx 61$ K, which could be explained by the influence of ion-beam etching and oxygen migration at SIO/YBCO interface. Some reduction of transition temperature T_{C_Nb}=8.4 K for Nb film also took place. The normal state resistivity of Nb/Au interface, studied earlier [20], gave $R_N A = 10^{-6}$ μΩcm^2, corresponding to a transparency $\Gamma \approx 1$. The averaged value of the normal resistance for four MS on one chip with SIO thickness d = 7 nm was $R_N A \approx 100$ μΩcm^2 at T = 4.2 K although the expected contribution from SIO film, taking experimental $\rho\, d = 7\ 10^3$ μΩcm^2, should be much higher [21]. This allows to conclude that a tunnelling through high-resistive barrier takes place. This explains the measured value of $R_N A$ and allows to argue that the tunnelling is the main mechanism of electrical transport through the SIO/Au interfaces in the MS with a total transparency $\Gamma = 3\ 10^{-5}$. Existence of zero-bias conductance peak (ZBCP), shown in figure 2b, demonstrates that the SIO/YBCO interface also is transparent enough and low-energy states occurred. So, the interface SIO/YBCO could be considered as N_{SO}/S, where N_{SO} is a normal metal with SOI, and S is a singlet superconductor. Taking into account the rise of conductance $G(V)$ at $V > 10$ mV at low temperatures which is inherent to tunnelling and could be caused by an existence of insulating barrier I between SIO and Au/Nb superconducting S' bilayer, the whole MS could be modelled as S'/I/N_{SO}/S.

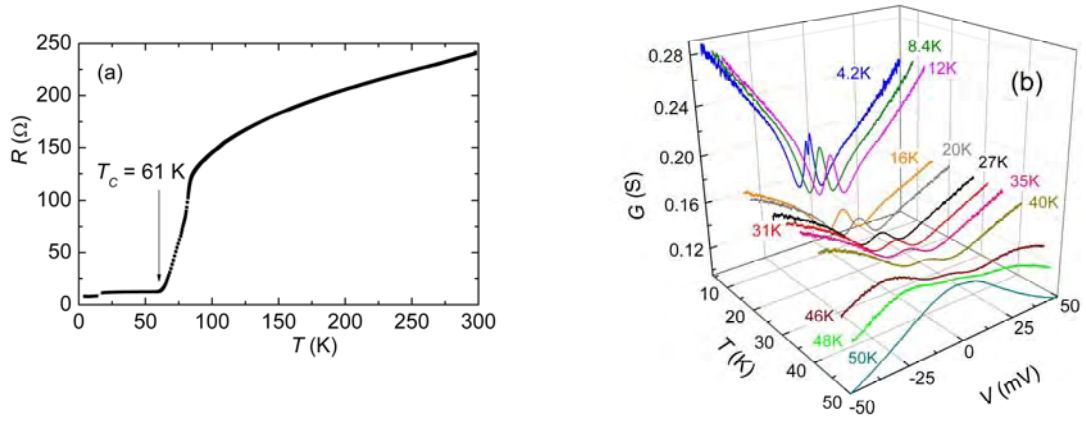

Figure 2. Temperature dependences of the resistance (a) of MS with size L= 40 μm and SIO film thickness d=7 nm. (b) *from* [21] Family of conductivity dependences $G(V)$ at T= 4.2 – 50 K.

The values of normal resistance R_N and critical current I_C were evaluated from the I-V curves (see figure 3a), using also the plots of differential resistance $R_D = dV/dI$. At temperatures near T_{C_Nb} the amplitudes of I_C were small and their values were determined from $R_D(I)$ as described in [21] since the influence of fluctuations resulted in "rounded" I-V curves. Temperature dependences of $I_C(T)$ and the voltage of singularity on $R_D(V)$ caused by the energy gap of the Nb electrode $V_\Delta(T)$ are given in figure 3b along with the BCS dependence of Nb gap.

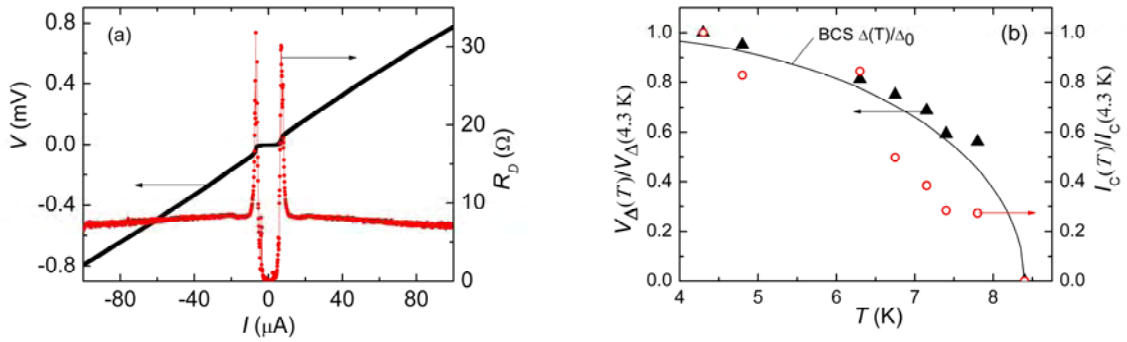

Figure 3. MS with L=40 μm and d=7 nm (a) I-V curve and differential resistance R_D=dV/dI versus current I. The critical current is determined by the local maxima of dV/dI. (b) Temperature dependences of the normalized critical current I_C and the normalized gap voltage V_Δ. A solid line is the normalized BCS dependence of the energy gap versus temperature. *From* [21].

In MS the s-wave Nb/Au superconducting electrode contacts via the SIO interlayer with the YBCO superconductor whose order parameter is described as a superposition of d-wave and s-wave components [22]. In comparison with Nb/Au/YBCO junctions [20] the MS with inserted SIO interlayer between YBCO and Au/Nb demonstrate about a twice reduction of the I_CR_N product. Note, superconducting current was absent in mesas with the interlayer made of any of ferromagnetic manganites $La_{0.7}Sr_{0.3}MnO_3$, $La_{0.7}Ca_{0.3}MnO_3$, or $LaMnO_3$ (all 3d materials) even at reduced temperatures below $T < 4.2$ K [23]. Thus, specific properties of SIO [24], which is 5d material with the strong SOI should be taken into account. According to experimental data [24] even a minor change in the oxygen content in SIO leads to a drastic change in the conductivity type at low temperature from activation to metallic. Oxygen migration at SIO/YBCO interface could play the decisive role for appearance of conducting part of SIO. This explains also evolution of conductivity $G(V)$ with temperature, demonstrating ZBCP up to T = 48 K, shown in figure 2b. Appearance of Andreev states at the interface of spin-singlet superconductor and a conductor with Rashba-type spin-orbit interaction may lead to removed spin degeneracy without the help of magnetic field [25]. Therefore, the effects [1-7, 18] predicted for a junction of spin-singlet YBCO superconductor and SIO with SOI could be relevant to our MS. When SOI is taken into account at the SIO/YBCO interface [26] a spin-triplet component of superconducting current may occur along with the long range proximity effect. Particularly, theoretical models [6, 7] for singlet-triplet conversion could be considered. Recently in ref. [27] was shown that with an increase of SOI the decay length of superconducting correlations can be significantly increased even in the absence of exchange field. In accordance to [7] in the case of large energy of SOI, comparable with Fermi energy E_{SO}~E_F, the decay length ξ of pairing amplitudes for the case of spin-triplet component becomes of order l_{SO}, the spin-orbit length. At the same time, theory [7] predicts enhancement for both spin-singlet and spin-triplet components with increase of SOI strength, and if E_{SO}=0 the triplet component is absent, but the singlet exists. Comparing critical current densities j_C for d=5nm and 7 nm, and assuming an exponential decay for characteristic length of superconducting current in MS, it gave an estimate for ξ~1 nm. However, a question of which components, singlet, triplet, or both survive over a few nm thick SIO in MS requires additional studies.

3.2. Magnetic field characteristics

Figure 4a shows magnetic-field dependence of superconducting critical current $I_C(H)$ with the maximum of I_C at H=0 for MS with d=5 nm, L=40 μm. During these set of measurements magnetic field was applied in-parallel of MS plane as shown in figure 1. Note, multi-turn amorphous mu-metal

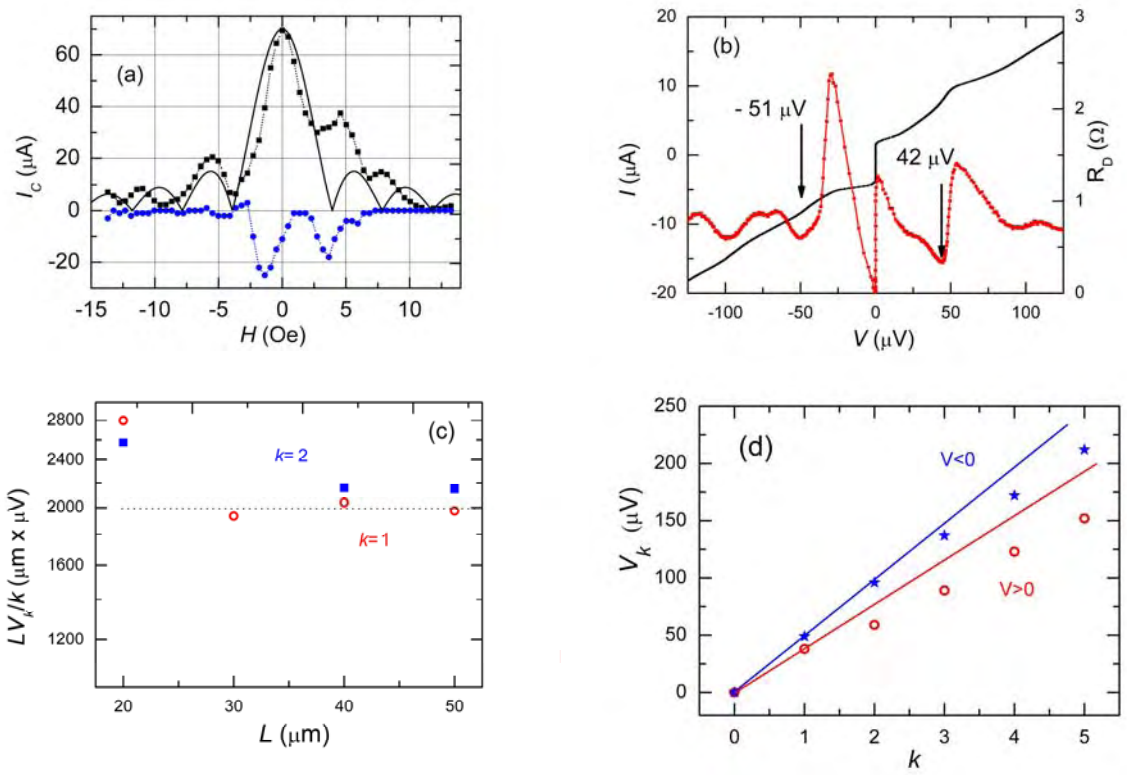

Figure 4. MS with L=40 μm and d=5 nm, Josephson penetration depth λ_J=170 μm, T=4.2 K. (a) Magnetic field dependences for critical current $I_C=(I_{C+}-I_{C-})/2$ – black symbols and $\Delta I_C=I_{C+}+I_{C-}$ – blue symbols, H-field was changed from right positive H point to negative. (b) I-V curve (black), and $R_D(V)$ (red) plotted at H= -2.7 Oe. Arrows point on Fiske resonance voltage positions for k=1. (c) The normalized by k the LV_k product vs. size L. Red symbols correspond to Fiske number k=1, blue to k=2. (d) Deviation of voltage positions of Fiske steps at positive (red symbols) and negative biasing (blue symbols). The straight lines show the expected dependences of Fiske resonance voltages, assuming linear rise of V_k with k, taking resonance voltage V_1 at k=1 as a fitting parameter.

shield reduced geomagnetic field about 10 times. Importantly, deviations from ordinary $I_C(H)$ dependence took place: an asymmetry of $I_C(H)$ relative the direction of applied magnetic field is seen. Moreover, critical current showed different values for positive I_{C+} and negative I_{C-} current biasing. This usually happens when Josephson junction has "large" size and the Josephson penetration depth λ_J is smaller than L [28]. In our experiment, on contrary, the MS has at least 4 times shorter L than Josephson penetration depth λ_J=170 μm. Figure 4a presents the difference between positive and negative critical currents (arithmetic sum) $\Delta I_C = I_{C+}+I_{C-}$ and the values of I_C defined as half amplitudes of superconducting currents at V=0: $I_C=(I_{C+}-I_{C-})/2$. Theoretical Fraunhofer dependence is also given in figure 4a. Calculated magnetic-field level which corresponds to the first minimum of the Fraunhofer pattern fits well to $H_1 = \Phi_0/\mu_0 d_J L \simeq 4$ Oe, $d_J=d+\lambda_{Nb}\mathrm{ctanh}(d_{Nb}/2\lambda_{Nb})+\lambda_{YBCO}\mathrm{ctanh}(d_{YBCO}/2\lambda_{YBCO})$, taking London penetration depths for YBCO and Nb at 4.2 K λ_{YBCO}=150 nm, λ_{Nb}= 90 nm, correspondingly. Note, MS with d=7 nm [21] had small critical current amplitudes and an existence of $\Delta I_C \neq 0$ could not been experimentally identified. Anomalous Josephson effect with phase shift requires specific conditions [29] e.g. it may happen in structures with spin bands splitting and presence of SOI [30]. In our experiment the level of applied magnetic field was much smaller for Zeeman splitting. At the same time another feature has been revealed in experiment, which hints on possible influence of magnon-

plasma wave interaction [31, 32]. Figure 4b shows an example of *I-V* curve and $R_D(V)$ dependence obtained at the fixed level of magnetic field. At voltages up to 200 μ*V* (not shown in figure 4b) differential resistance $R_D(V)$ demonstrates oscillations which could be explain by Fiske resonances at $V_k=k(\mathrm{h}/2\mathrm{e})c'/2L$, $c'=c(d/\varepsilon\, d_J)^{1/2}$ is Swihart velocity. Changing the MS size the voltage positions of Fiske resonances changed as shown in figure 4c. Minor variation of expected V_kL products with changing *L* is seen, showed for the 1st and 2nd Fiske steps. At the same time the difference in V_{+1} and V_{-1} marked by arrows is seen well on $R_D(V)$ in figure 4b. An asymmetry has been observed also for higher *k*, as shown in figure 4d. Theoretical prediction of an asymmetry and deviation from ordinary Fiske resonance voltage positions were made in [31, 32] for the case of ferromagnetic insulator (IF, or IFI barriers) were mutual interaction of spin waves and plasma waves occurs. Spin waves in antiferromagnetic insulators are less studied, however their existence were examined in antiferromagnetic thin films [33], and antiferromagnetic spin dynamics in SIO was reported in ref. [34]. Fiske resonances were reported for Josephson junctions with metallic ferromagnets in IF barrier [35] without any deviation in V_k positions from ordinary theory [28]. A minor shift was noticed in ref. [36] which, however, could be explained by an influence of electromagnetic surrounding [37]. In our experimental case deviations are rather more pronounced. Furthermore, estimated from Fiske resonance position V_1 the plasma frequency f_P~25 GHz gives high value of dielectric constant ε~ 40 – 45, which does not contradict to values experimentally measured for SIO crystals [38] at somewhat higher temperatures than in our experiment and were explained by existence Mott band and strong SOI properties [39] in Sr_2IrO_4.

3.3. Microwave characteristics of MS

The information on high frequency properties of MS could be obtained from the dynamics of Shapiro steps by varying the power of microwave irradiation [20, 40]. Since the characteristic frequency for MS $f_C=(I_CR_N)2\mathrm{e}/\mathrm{h}$ (h is Planck's constant) lies in GHz-range, the measurements were carried out in mm-wave frequency band. Figure 5a shows the voltage dependence of $R_D=\mathrm{d}V/\mathrm{d}I$ of MS with d=7 nm and L=40 μm measured at the fixed level of applied microwave power at frequencies f_e=38 GHz and f_e=50 GHz demonstrating Shapiro steps arising due to synchronization between Josephson oscillations and the external microwaves at voltages $V_{\mathrm{n,m}}=(n/m)\mathrm{h}f_e/2\mathrm{e}$. Very well correspondence to Josephson voltage-frequency relation has been registered as shown in figure 5b. The fractional Shapiro steps have been also registered which may indicate the presence of the second harmonic in current-phase relation (CPR) $I_{C2}\neq 0$. Figure 5c shows dependence of the fractional (half-integer) $i_{1/2}=I_{C2}/I_C$ (n=1, m=2) Shapiro step from normalized microwave current $a=I_{MW}/I_C(0)$ at f_e=50 GHz. The theoretical dependence of $i_{1/2}(a)$ was calculated for different values of $q=I_{C2}/I_C$, using the modified RSJ model [20, 40]. Experimental data demonstrated well defined local maxima for $i_1(a)$ at $a\approx 20$ and a minor one at $a\approx 80$. Note, for $q>0$ the minima of theoretical function $i_1(a)$ do not reach $i_1=0$ (see data given in [21]), but the $i_{1/2}(a)$ does. Deviation of experimental $i_1(a)$ dependence from theoretical could be attributed to presence of higher harmonics in CPR, as well by the impact of enhanced strong non-stationary processes which are not considered in the model [20, 40]. Taking the maximal amplitude of experimental dependence $i_{1/2}(a)\approx 0.3$ the best fit for half-integer Shapiro step corresponds to the theoretical function for q=0.3. The *d*-wave component of the YBCO superconducting order parameter promotes an unconventional superconducting CPR of the junction with the 2nd harmonic component [20]. The estimation of contribution of the second harmonic caused by the d-wave symmetry for a S/D junction (S – s-wave superconductor, D – d-wave superconductor in *c*-axis direction) with the same electrical parameters as the discussed MS gives second harmonic amplitude $I_{C2}\approx 20$ nA for transparency $\mathcal{T}=2\cdot 10^{-4}$, Δ_{Nb}/e=0.8 mV and R_N=7.1 Ω at T=4.2 K. Using the theoretical dependence for ratio I_{C1}/I_C versus q [20, 41] and the estimated "d-wave" contribution of I_{C2}, we obtain a negligibly small $q\approx 3\ 10^{-3}$ for S/D junction. Figure 5d demonstrates *I-V* curve and voltage sependence of the synchronous detector response at f_e=50 GHz for MS with d=5 nm, L=40 μm. As seen from figure 5d strong singularities caused by Fiske resonances in MS with d=5 nm do not allow to conclude whether

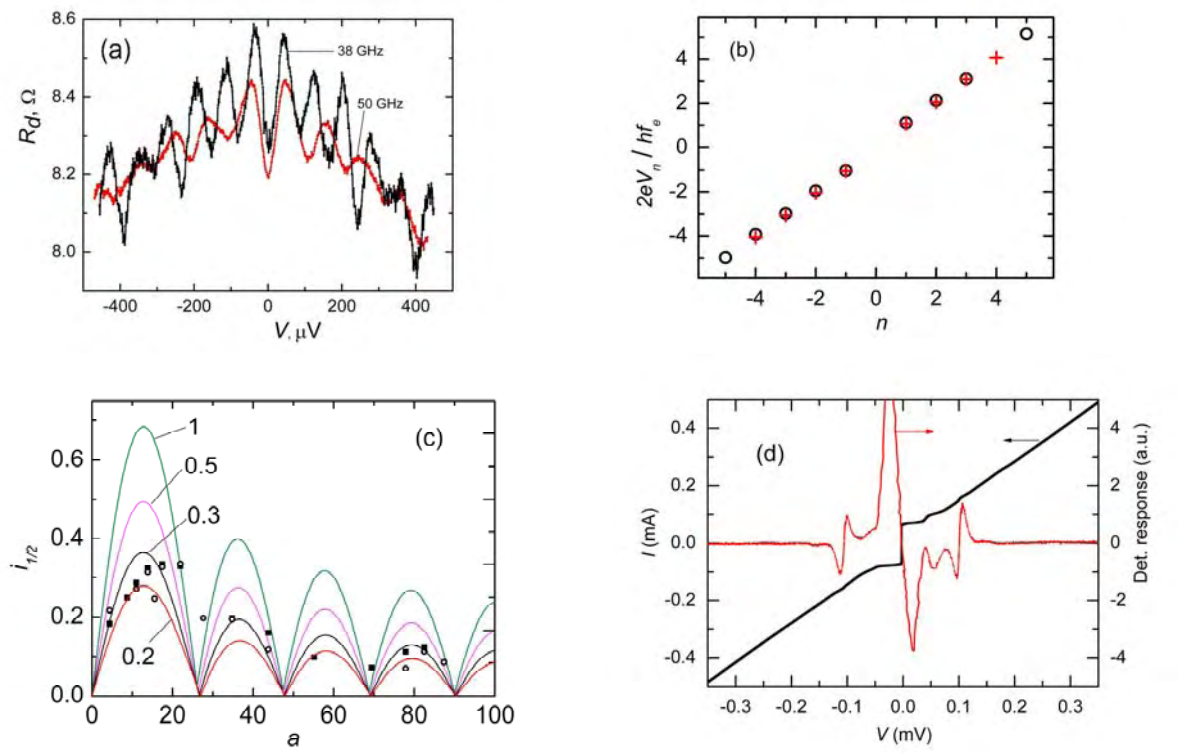

Figure 5. AC Josephson effect in MS with L=40 μm at T=4.2 K. (a) Dependences of differential resistance $R_D(V)$ of MS with d=7 nm at 38 GHz (black), 50 GHz (red). (b) Voltage-frequency Josephson ratio vs. Shapiro step number n: black symbols f_e=38 GHz, red - 50 GHz. (c) *from* [21] Normalized amplitudes of n=1/2 Shapiro steps $i_{1/2}=I_{C2}(a)/I_C(0)$. Theoretical curves are given for q=0.2, 0.3, 0.5, 1 and McCumber parameter β_C=1. (d) I-V curve and detector response at 50 GHz for MS with d=5 nm.

there exists a fractional Shapiro step with a drop in $R_D(V)$ function at the voltage $V_{n,m.}$ corresponding to the experimental frequencies f_e.

The deviation of CPR from sinusoidal may originate due to appearance of low energy states at the SIO/YBCO interface, related to the coherent Andreev reflections [7, 18, 42]. Indeed, the MS demonstrated the zero-bias conductivity peak at temperatures T=4.2 K as well at temperatures $T>T_{C\_Nb}$ which could be associated with the low energy states. At the same time a tunneling type conductivity is seen at higher voltages V>10 mV at low temperatures along with the asymmetry of $G(V)$ dependence. Note, the theoretical simulation [18] shows that the interface of cuprate superconductor with the SIO could exhibit both helical Majorana fermions and zero-energy flat edge states. However, the origin of the ZBCP and the asymmetry of $G(V)$ in the MS require additional studies.

4. Conclusions

In conclusion, Nb/Au/Sr_2IrO_4/$YBa_2Cu_3O_x$ mesa-structures with epitaxial bilayer of Sr_2IrO_4 and $YBa_2Cu_3O_x$ films have been fabricated. The superconducting current for the thickness d=5 and 7 nm of Sr_2IrO_4 interlayer has been registered. The critical current of the mesa-structure increased with decreasing temperature similarly as the voltage of the energy gap singularity of Nb film. The zero-bias conductance peak has been observed. Under influence of magnetic field the critical current $I_C(H)$ dependences showed Fraunhofer-like pattern indicating absence of pinholes, supported also by oscillating with microwave power Shapiro steps. Fiske resonances were registered for samples with d=5 nm. Under electromagnetic radiation at millimetre wave frequency band, the Shapiro steps

including the fractional ones were observed for mesas with *d*=7 nm, indicating the deviation of the current-phase relation from the sinusoidal and the presence of the second harmonic, which could not be explained solely by impact of d-wave symmetry of *c*-oriented YBCO electrode.

Acknowledgments
The authors gratefully acknowledge A.V. Zaitsev, L.V. Filippenko, for the help and useful discussions. Microwave characteristics were obtained using equipment USU 352529 at IRE RAS. The work was partially supported by the RFBR project 19-07-00274, and Program of Russian Academy of Sciences "Quantum effects in condensed matter at low temperatures".

References
[1] Eschrig M 2015 *Rep. Prog. Phys.* **78** 104501
[2] Linder J and Robinson J W A 2015 *Nat. Phys.* **11** 307
[3] Bergeret F S and Tokatly I V 2014 *Phys. Rev. B* **89**,134517
[4] Konschelle F, Tokatly I V and Bergeret F S 2014 *Eur. Phys. J. B* **87** 119
[5] Bergeret F S, Volkov A F and Efetov K B 2005 *Rev. Mod. Phys.* **77** 1321
[6] Bobkova I V and Bobkov A M 2017 *Phys. Rev. B* **95** 84518
[7] Reeg C R and Maslov D L 2015 *Phys. Rev. B* **92** 134512
[8] Sau J D, Lutchyn R M, Tewari S and Das Sarma S 2010 *Phys. Rev. Lett.* **104** 040502
[9] Suominen H J, Danon J, Kjaergaard M, Flensberg K, Shabani J, Palmstrøm C J, Nichele F and Marcus C M 2017 *Phys. Rev. B* 95 035307
[10] Sun D and Liu J 2018 *Phys. Rev. B* **97** 035311
[11] Moon S J, et al. 2008 *Phys. Rev. Lett*. **101** 226402
[12] Witczak-Krempa W, Chen G, Kim Y B and Balents L 2014 *Annu. Rev. Condens. Matter Phys.* **5** 57
[13] Gim Y, Sethi A, Zhao Q, Mitchell J F, Cao G and Cooper S L 2016 *Phys. Rev. B* **93** 024405
[14] Hikino S-i 2018 *J. Phys. Soc. Japan*, **87** 074707
[15] Ovsyannikov G A, Grishin A S, Constantinian K Y, Shadrin A V, Petrzhik A M, Kislinskii Yu V, Cristiani G and Logvenov G 2018 *Phys. Solid State* **60** 2166
[16]. Petrzhik A M, Christiani G, Logvenov G, Pestun A E, Andreev N V, Kislinskii Yu V and Ovsyannikov G A 2017 *Tech. Phys. Lett*. **43** 554
[17] Wang H Yu S-L and Li J-X 2015 *Phys. Rev. B* **91** 165138
[18] Chen Y and Kee H-Y 2018 *Phys. Rev. B* **97** 085155
[19] Satchell N and Birge N O 2018 *Phys. Rev. B* **97** 214509
[20] Komissinskiy P, Ovsyannikov G A, Constantinian K Y, Kislinski Y V, Borisenko I V, Soloviev I I, Kornev V K, Goldobin E and Winkler D 2008 *Phys. Rev. B* **78** 024501
[21] Petrzhik A M, Constantinian K Y, Ovsyannikov G A, Zaitsev A V, Shadrin A V, Grishin A S, Kislinski Yu V, Cristiani G and Logvenov G 2019 *Phys. Rev. B* **100** 024501
[22] Komissinski P V, Il'ichev E, Ovsyannikov G A, Kovtonyuk S A, Grajcar M, Hlubina R, Ivanov Z, Tanaka Y, Yoshida N and Kashiwaya S 2002 *Europhys. Lett.* **57** 585
[23] Petrzhik A M, Ovsyannikov G A, Shadrin A V, Konstantinyan K Y, Zaitsev A V, Demidov V V and Kislinskii Yu V 2011 *J. Exp. Theor. Phys.* **112** 1042
[24] Korneta O B, Qi T, Chikara S, Parkin S, De Long L E, Schlottmann P and Cao G 2010 *Phys Rev. B* **82** 115117
[25] Reynoso A A, Usaj G, Balseiro C A, Feinberg D and Avignon M 2012 *Phys. Rev. B* **86** 214519
[26] Horsdal M and Hyart T 2017 *Sci. Post Phys.* **3** 041
[27] Lu Y and Heikkilä T T 2019 arXiv: 1905.11135
[28] Barone A and Paternò G 1982 *Physics and Applications of the Josephson Effect* (Wiley, NY)
[29] Silaev M A, Tokatly I V and Bergeret F S 2017 *Phys. Rev. B* **95** 184508
[30] Calder S 2018 *Phys. Rev. B* **98** 220402(R)
[31] Mai S, Kandelaki E, Volkov A F and Efetov K B 2011 *Phys. Rev. B* **84** 144519

[32] Hikino S-i, Mori M, Takahashi S and Maekawa S 2011 *J. Phys. Soc. Jpn*. **80** 074707
[33] Boardman A D, Nikitov S A and Waby N A 1993-II *Phys. Rev. B* **48** 13602
[34] Bahr S, Alfonsov A, Jackeli G, Khaliullin G, Matsumoto A, Takayama T, Takagi H, Büchner B and Kataev V 2014 *Phys. Rev. B* **89** 180401(R)
[35] Wild G, Probst C, Marx A and Gross R 2010 *Eur. Phys. J.* B **78** 509
[36] Pfeiffer J, Kemmler M, Koelle D, Kleiner R, Goldobin E, Weides M, Feofanov A K, Lisenfeld J and Ustinov A V 2008 *Phys. Rev. B* **77** 214506
[37] Monaco R, Costabile G and Martuccielle N 1995 *J. Appl. Phys*. **77** 2073
[38] Chikara S, Korneta O, Crummett W P, DeLong L E, Schlottmann P and Cao G 2009 *Phys. Rev. B* **80** 140407R
[39] Hu J 2008 *Phys. Rev. Lett.* **100** 077202
[40] Kornev V K, Karminskaya T Y, Kislinski Y V, Komissinki P V, Constantinian K Y and Ovsyannikov G A 2006 *Physica C* **435** 27
[41] Goldobin E, Koelle D, Kleiner R and Buzdin A 2007 *Phys. Rev. B* **76** 224523
[42] Chiu C-K and Das Sarma S 2019 *Phys. Rev. B* **99** 035312